The Intercontinental Journal of
Internal Medicine

DOI: 10.51271/ICJIM-0042

Original Article

# Evaluation with spiral computed tomography angiography after intravascular stent application in atherosclerotic renal artery stenosis

Hasibe Gökçe Çınar[1], Erhan Turgut Ilgıt[2], Mehmet Araç[2]

[1]Department of Radiology, Ankara Etlik City Hospital, Ankara, Turkiye
[2]Department of Radiology, Faculty of Medicine, Gazi University, Ankara, Turkiye

**Cite this article:** Gökçe Çınar H, Erhan Ilgıt T, Araç M. Evaluation with spiral computed tomography angiography after intravascular stent application in atherosclerotic renal artery stenosis. *Intercont J Int Med.* 2024;2(4):82-88.

**Corresponding Author:** Hasibe Gökçe Çınar, hgecinar@yahoo.com

**Received:** 02/06/2024 ◆ **Accepted:** 05/08/2024 ◆ **Published:** 30/10/2024

## ABSTRACT

**Aims:** With the development of spiral scanning, computed tomography angiography (CTA) is preferred over conventional angiography in many vascular applications. Reduced respiratory and motion artifacts and ability to catch arterial phase during one inspiration are the advantages of spiral CTA. Our aim in this study is to evaluate the value of spiral CTA in demonstrating stent integrity, stent patency, and renal artery/stent relationship after renal artery stenting.

**Methods:** 15 patients (12 male and 3 female) who had renal artery metallic stents were included in this study. Systolic and diastolic blood pressure and creatinine values of the patients were measured before and after the stent. Patients were examined by CTA after renal artery stenting. In renal artery segments with renal artery stenosis and stenting on CTA; stent diameter, stent length, integrity, luminal contrast enhancement and intraluminal calcification were evaluated with 1 mm axial reconstructed images and "post-process" techniques multiplanar reformat (MPR), maximum intensity projection (MIP), shaded surface display (SSD), and virtual intravascular endoscopy (VIE).

**Result:** Of the stenosis in which stents were placed, 1 was located in the proximal renal artery, 4 were in the mid-renal artery, and 10 were ostial. The whole stent was visualized in 8 cases. Among the MPR images, the axial plane was the best to depict the lumen in 13 cases. The stent lumen was best visualized on oblique MPR images in the axial plane. The visibility of the stent lumen decreased in MIP images with increased slice thickness. In cases where stenosis was considered due to intimal hyperplasia within the stent, no stenotic appearance was observed on MPR and MIP images. In all patients, stent and wall calcifications were observed separately from the contrast medium on MPR and MIP images. On SSD images, the stent could not be distinguished from contrast material and vascular wall calcifications in all patients. In VIE images, the renal artery ostium and the stent were viewed from the aortic lumen in all patients. The stent was observed as patent in 14 cases. In one case, occlusion was demonstrated proximal to the stent.

**Conclusion:** Spiral CTA is a noninvasive procedure in evaluating the integrity of the stent, stent patency and renal artery/stent relationship after renal artery stenting.

**Keywords:** Spiral CT Angiography, renal artery stenosis, renal artery stenting

## INTRODUCTION

Atherosclerotic renal artery stenosis (RAS) is the most common cause of secondary hypertension and may lead to resistant hypertension, progressive deterioration of renal function, and cardiac destabilization syndromes, including pulmonary edema, acute coronary syndrome and heart failure, despite adherence to guideline-directed medical treatment.[1] Due to the variable prevalence of RAS, radiological methods are crucial for diagnosis. Conventional angiography (DSA) is considered the gold standard in diagnosis. Its greatest advantage is that it allows for widely accepted therapeutic interventions, such as percutaneous transluminal angioplasty and stent placement, to be performed immediately after the diagnostic examination.[2]

Color Doppler ultrasound of the renal artery plays a significant role in diagnosing RAS due to its non-invasive and repeatable nature. However, this method requires a long examination time to visualize the main renal artery. A previous study determined that Doppler ultrasound examination for predicting RAS offered 82.90% sensitivity, 70% specificity, an 85% positive predictive value, and a 66.7% negative predictive value.[3] The use of magnetic resonance angiography (MRA) as a non-invasive method has also been increasing in recent years. In patients with a high clinical suspicion of RAS, MRA is 87% sensitive in the detection of >50% stenosis. However, MRA is relatively nonspecific compared with CA and results

in significant overestimation of RAS in nearly one third of patients.[4,5]

With the development of spiral scanning, computed tomography angiography (CTA) has increasingly become the preferred method over DSA in many vascular applications.[6,7] The most important advantage of spiral CTA is its ability to minimize artifacts caused by respiration and patient movement, while capturing arterial phase data of intravenously administered contrast material within a single breath-hold. Significant advancements in spiral CTA have been achieved through post-processing techniques such as multiplanar reformat (MPR), maximum intensity projection (MIP), shaded surface display (SSD), and virtual intravascular endoscopy (VIE).[8] By selecting appropriate scanning parameters and post-processing techniques, spiral CTA has found widespread use in the evaluation of various pathologies, including aortic aneurysms and dissections, pulmonary embolism, and RAS.[9-11]

The aim of this study is to investigate the efficacy and adequacy of spiral CTA in demonstrating stent integrity, patency, and the relationship between the stent and renal artery following renal artery stenting.

## METHODS

This cross-sectional study was conducted at the Radiology Department of Gazi University Faculty of Medicine from August 1996 and March 2001. The study was produced from a thesis before 2020 and institutional approval was received. All procedures were carried out in accordance with the ethical rules and the principles of the Declaration of Helsinki.

A total of 15 patients who underwent intravascular metallic stent placement in the renal artery due to RAS were included in the study. The patients' systolic and diastolic blood pressure values, as well as creatinine levels, were recorded before and after stent placement. Post-stent follow-up spiral CTA examinations were performed on the first day and at the 44th month after stent placement. Three patients underwent two spiral CTA examinations and one DSA. The spiral CTA was performed using a HiSpeed CT/i (GE Medical Systems, Milwaukee, USA) device. Initial images were used to determine the localization of the renal stents and the scanning area. The CTA was performed after administering 100-130 cc of non-ionic contrast material at a rate of 2.5-3 cc/sec via an automatic injector, through a 20G intravenous cannula in the antecubital vein, with a minimum of 100 cc (1.5 cc/kg). The scanning duration was approximately 19 seconds. The renal artery segments with RAS and stent placement were recorded.

Stent diameter and length were measured to assess the presence of stenosis. Maximum diameter measurements were taken from 1-mm axial reformatted images of the stent from the location where the stent was best visualized on standard axial images. Stent length was measured using oblique reformatted images, referencing the stent plane.

In all patients, MPR, MIP, SSD, and VIE images were generated using standard software. Stent integrity, lumen, presence of intraluminal calcification, and stenosis were evaluated and compared using MPR and MIP images. SSD images were used to assess the stent, intraluminal contrast enhancement, and wall calcifications, while VIE evaluated the visibility of the renal artery ostium, stent patency, and the lumens of renal artery segments distal and proximal to the stent.

The stents were expanded and released according to the manufacturer's recommendations by inflating the balloon at the nominal pressure, assuming they reached the desired diameter. Measurements were taken before and after stent deployment, and these two measurements were compared.

Density measurements were performed in all patients to evaluate renal artery and aortic contrast enhancement, as well as stent patency. For density measurements, a section where the lumen was best visualized on 1-mm reconstructed standard axial images was selected. Densities were measured in Hounsfield units (HU) from a 5 $mm^2$ area at the midsection of the abdominal aorta, the segment of the renal artery distal to the stent, and the contralateral renal artery.

In all cases, the kidney size, contrast enhancement, and cortical thickness were evaluated using the 1-mm reconstructed standard axial images.

### Statistical Analysis

All data were analyzed with Microsoft Excell program v.10 (Microsoft Corporation, Redmond, WA, USA). Numerical data are given as mean and standard deviation (SD). Categorical variables are given as numbers and percentages.

## RESULTS

The study included 15 patients, 12 men and 3 women, aged between 40 and 70 years (mean age 58.0±10.4 years). Fourteen of the patients were hypertensive, and one was normotensive. The mean pre-procedural systolic blood pressure of the hypertensive patients was 161.6±20.1 mmHg, and the mean diastolic blood pressure was 95.3±10.2 mmHg. In the follow-up after stent placement, the mean systolic blood pressure was measured as 140.0±22.9 mmHg, and the mean diastolic blood pressure as 86.0±20.2 mmHg. The mean serum creatinine level was 1.4±0.5 mg/dl before the procedure and 1.2±0.4 mg/dl after the procedure. Six patients had impaired renal function before the procedure (creatinine >1.4 mg/ml). In four of these patients, a decrease in creatinine levels was observed after the procedure, while in two patients, elevated creatinine levels persisted.

Of the stenoses treated with stent placement, one was located in the proximal renal artery, four in the mid-renal artery, and ten in the ostial. In eight patients, the stent was fully visualized, whereas in seven patients, it was not fully visualized. In 13 cases, the optimal plane for visualizing the lumen was determined to be axial on the MPR images. In one case, due to artifacts caused by the stent, the lumen was only partially visible in the axial plane. In another case, the best visualization of the stent integrity was obtained in the sagittal and coronal planes due to the angle formed between the stent and the aorta (Figures 1, 2).

In MIP images obtained with increased slice thickness, the best plane for visualizing the stent lumen in 10 cases was the axial plane with thicknesses between 1.5 and 2.1 mm. In 4 cases, the stent lumen was only partially visible in the axial plane with thicknesses between 1.2 and 2.1 mm. As a result, the stent lumen was best visualized in the oblique MPR images in the axial plane. In the MIP images with increased slice thickness, the visibility of the stent lumen decreased as the slice thickness increased.

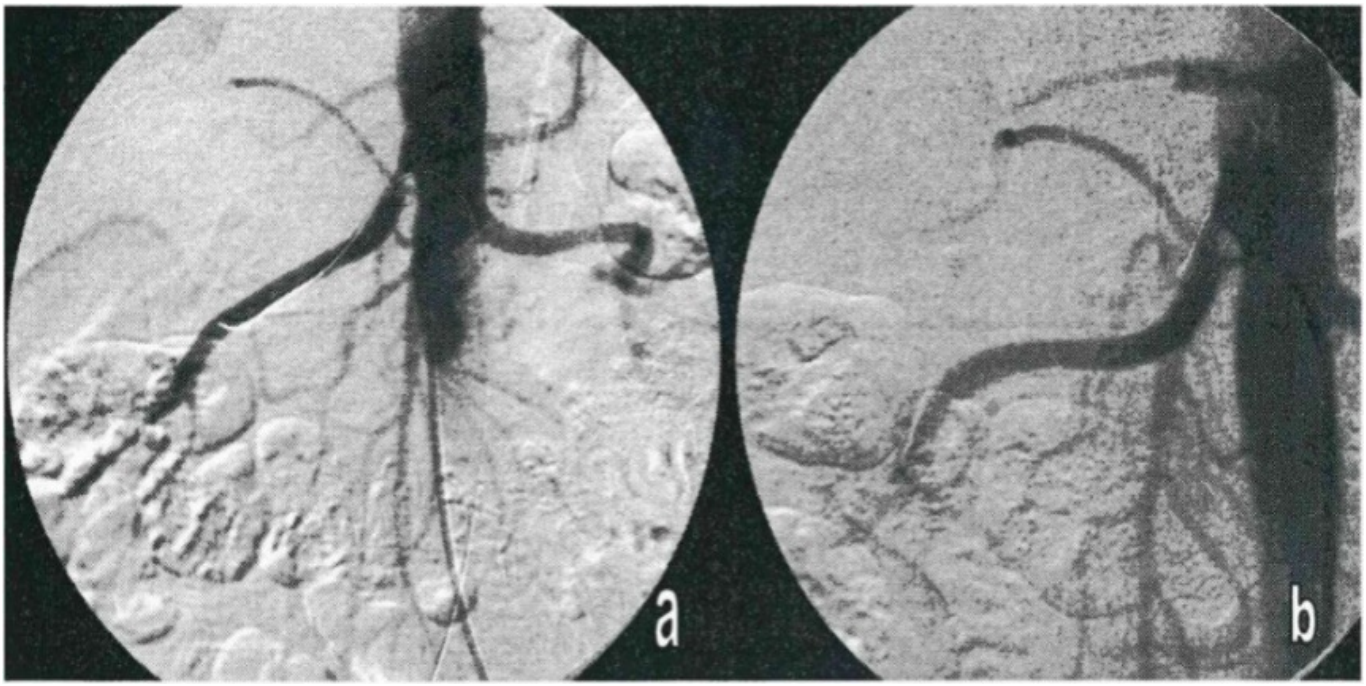


**Figure 1.** (a) A 75% ostial stenosis in the right renal artery is shown. (b) Following stent placement, this segment appears patent (open and unobstructed)

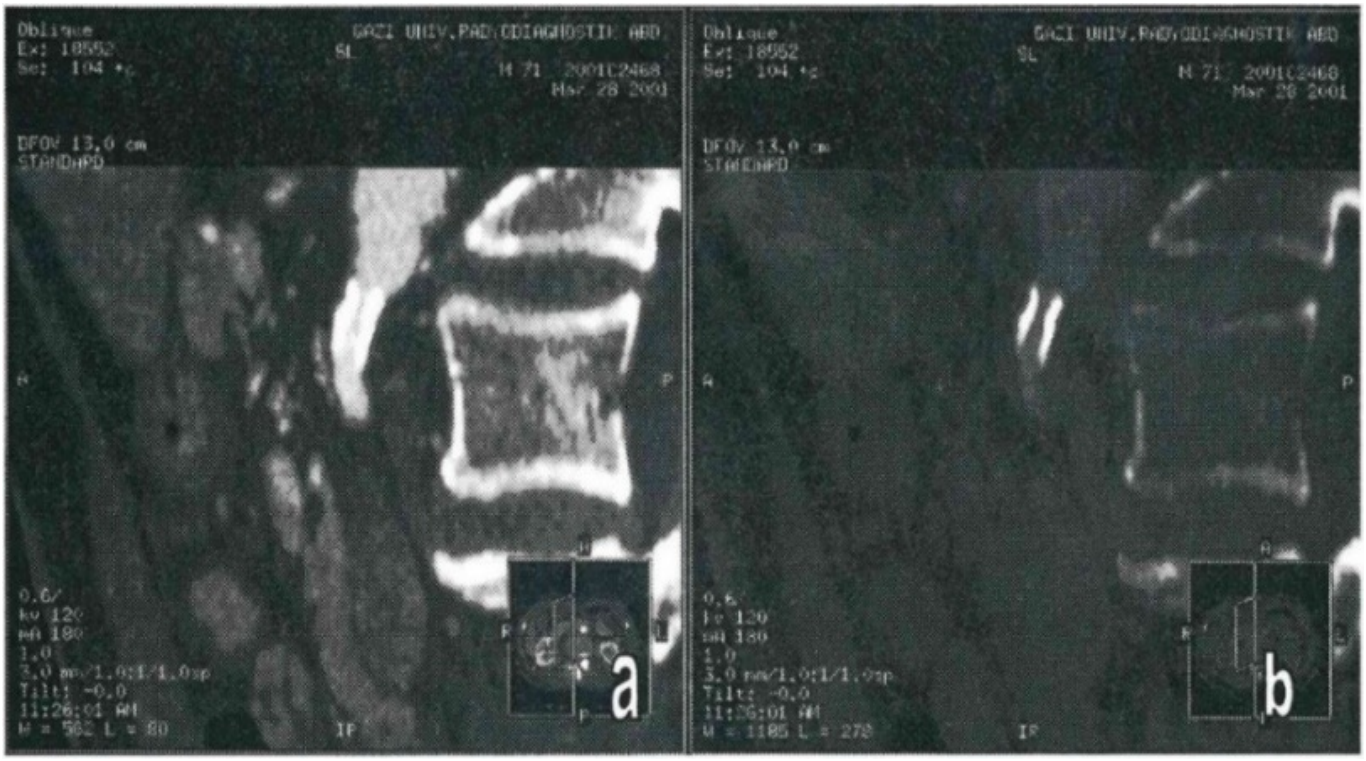


**Figure 2.** In the same case, a 0.6 mm thick oblique MPR image obtained from the sagittal plane, with the stent used as a reference (a: windowing for vascular structures, b: windowing for the stent), shows the stent as patent

In the evaluation of all the obtained images, the renal artery and stent level were observed to be patent in 14 cases. However, in one case, an occlusion was detected in the proximal segment of the renal artery on the stent side, and no contrast enhancement was observed in the stent lumen (Figures 3-7).

In one patient, oblique MPR images obtained in the axial plane revealed stenosis in the renal artery just proximal to the stent. In cases suspected of stenosis due to in-stent intimal hyperplasia, no stenotic appearance was observed in the MPR and MIP images.

In all patients, the stent was visualized separately from the contrast material in the MPR and MIP images. Vascular wall calcifications were separately visualized from the contrast material in the MPR and MIP images of 13 patients. In all patients, the vascular structures distal to the stent were displayed on MIP images in accordance with the degree of contrast enhancement. The continuity of the vascular structures was best observed in MIP images with thicknesses ranging from 7.3 to 10.7 mm.

With SSD, the stent could not be differentiated from the contrast material and vascular wall calcifications in any of the

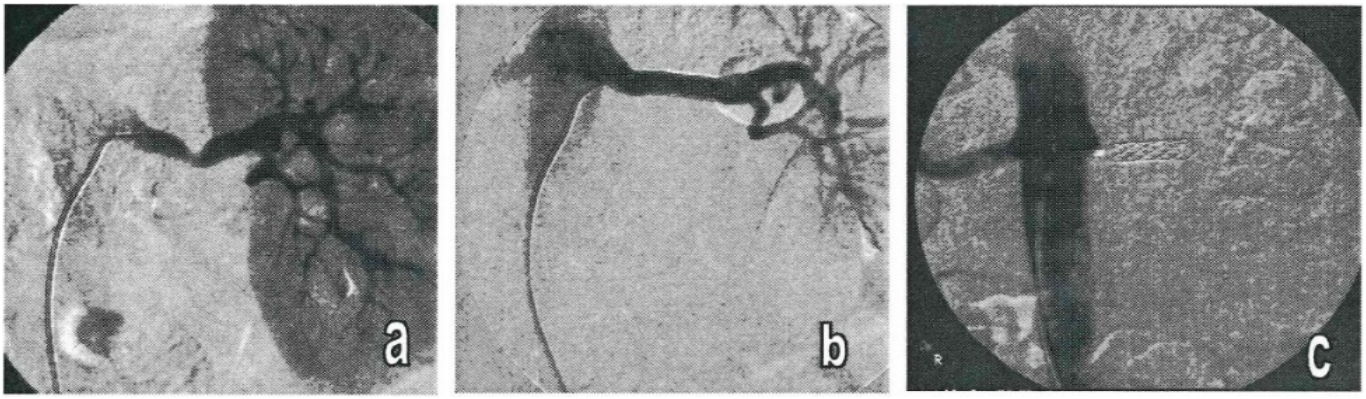


**Figure 3.** (a) A 70% stenosis in the midsection of the left renal artery, (b) stent placement following dissection that developed after balloon dilation, (c) 4.5 years later, angiographic follow-up showing occlusion in the left renal artery

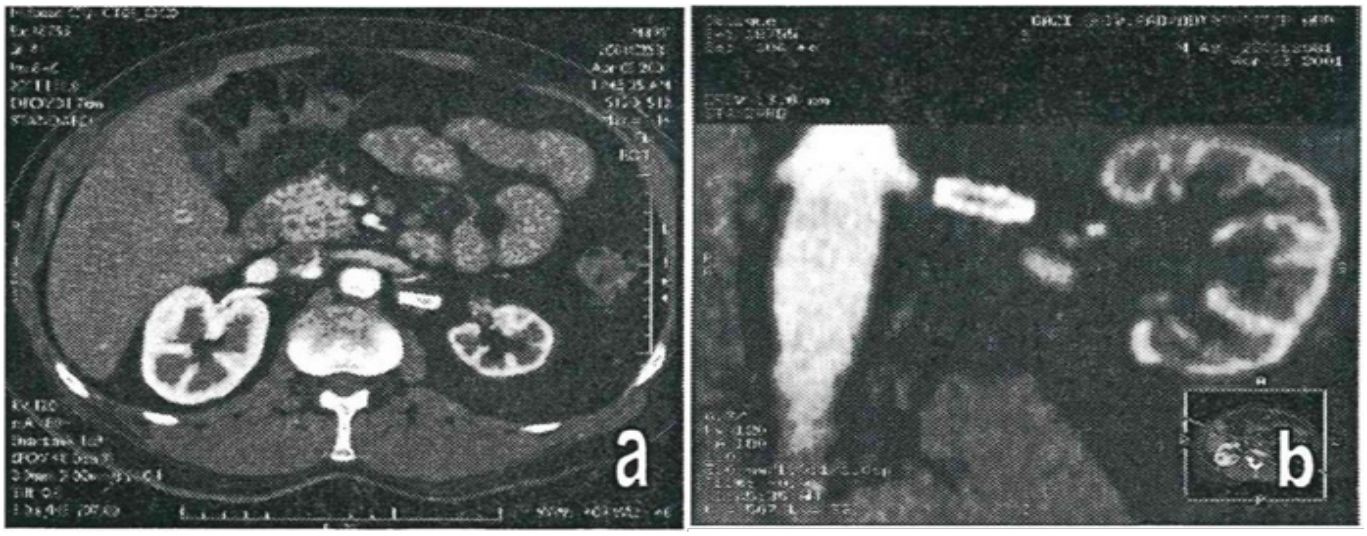


**Figure 4.** (a) In the same case, 4.5 years later, the spiral CTA follow-up shows a 1 mm reconstructed standard axial image obtained from volumetric data, and (b) a 0.7 mm thick MPR image in the coronal plane demonstrates a reduction in the size of the left kidney (long axis: 60 cm) and cortical thinning. Both kidneys are visible in the nephrogram phase

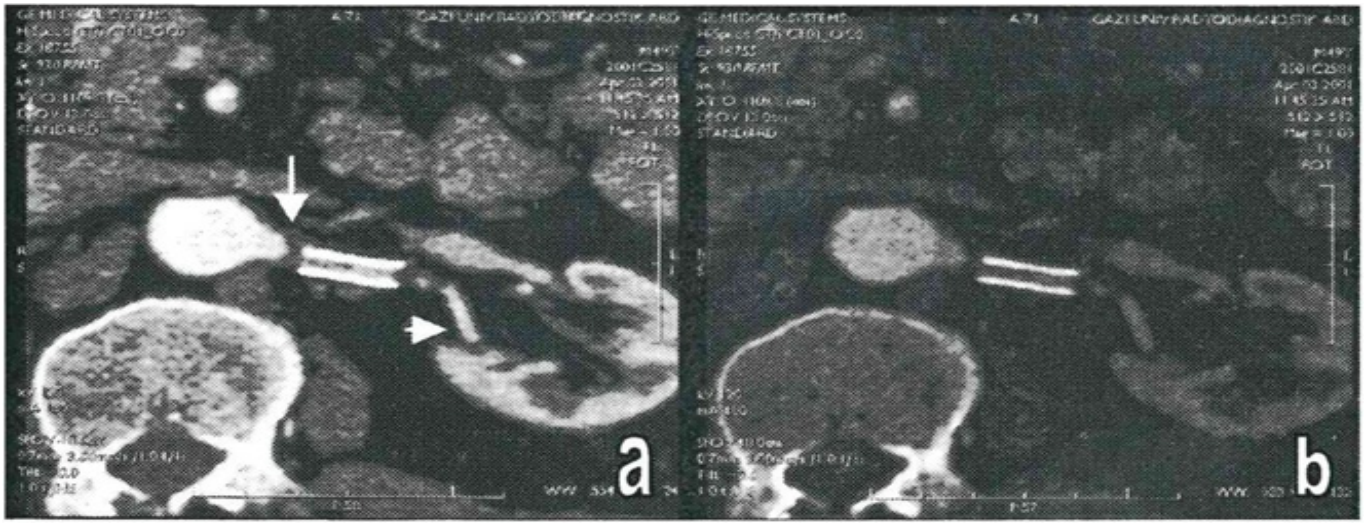


**Figure 5.** In the same case, oblique MPR images (0.7 mm thick) obtained from the axial plane using the stent as a reference (a: windowing for vascular structures, b: windowing for the stent) show: (a) an occlusion (arrow) in the proximal left renal artery with no opacification of the stent lumen, and (b) opacification in the segmental branches of the renal artery distal to the stent (arrowhead). Additionally, cortical thinning in the left kidney is noted

patients. However, the stent was observed to be wider than the renal artery at its localization site.

In VIE images, the threshold value was selected between 97 and 206. In all patients, the renal artery ostium and the stent were visualized from the aortic lumen. The stent lumen and the area distal to the stent were evaluated. The stent was patent in 14 cases, while occlusion was observed proximal to the stent in one case. In all patients, the stent lumen was observed with contour irregularities.

In one patient, bilateral accessory arteries were observed in both MIP and SSD images. Additionally, in 3 cases where stenosis was detected in the contralateral renal artery on

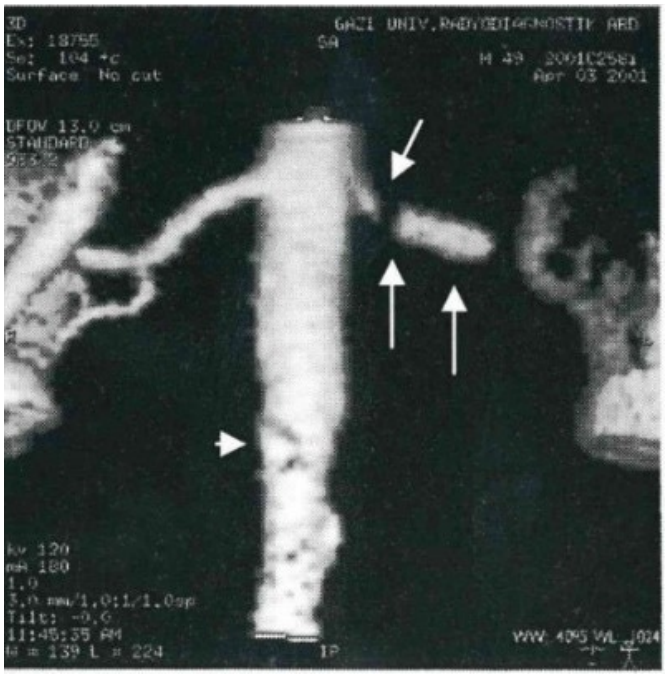

**Figure 6.** In anteriorly viewed SSD images of the same case, the right renal artery is seen to be patent, while an occlusion (arrow) is visible in the proximal left renal artery. Due to the density of the stent (double arrow), intraluminal contrast material, and aortic wall calcification exceeding the selected density threshold, they cannot be distinguished from each other. Aortic wall calcification is partially visible as contour irregularities (arrowhead)

angiography, the stenotic segment was shown in both MIP and SSD images (Figure 8). In the patient with stent occlusion, density measurements taken from the area adjacent to the distal end of the stent were found to be significantly lower. In all other cases, no significant differences in density values were detected.

## DISCUSSION

With the advancement of spiral CTA, volumetric data can now be obtained without respiratory artifacts during the peak arterial vascular opacification following peripheral contrast material injection, allowing for the creation of two-dimensional (2D) and three-dimensional (3D) images.[12] When the reconstruction interval is selected to be smaller than the collimation and three images are reconstructed per rotation, sufficient images for 3D diagnosis can be generated. As the interval decreases, the partial volume effect is also reduced, facilitating the visualization of small vessels.[13] Additionally, reducing the reconstruction interval will increase the number of images that make up the scanning volume, as well as the time required for post-processing and evaluation, and the storage space needed for these images. In our study, a reconstruction interval of 1 mm was used for all cases.[14,15]

Narrow collimation increases both axial and longitudinal resolution. However, it also increases pixel noise while reducing the distance scanned within the procedure time. The

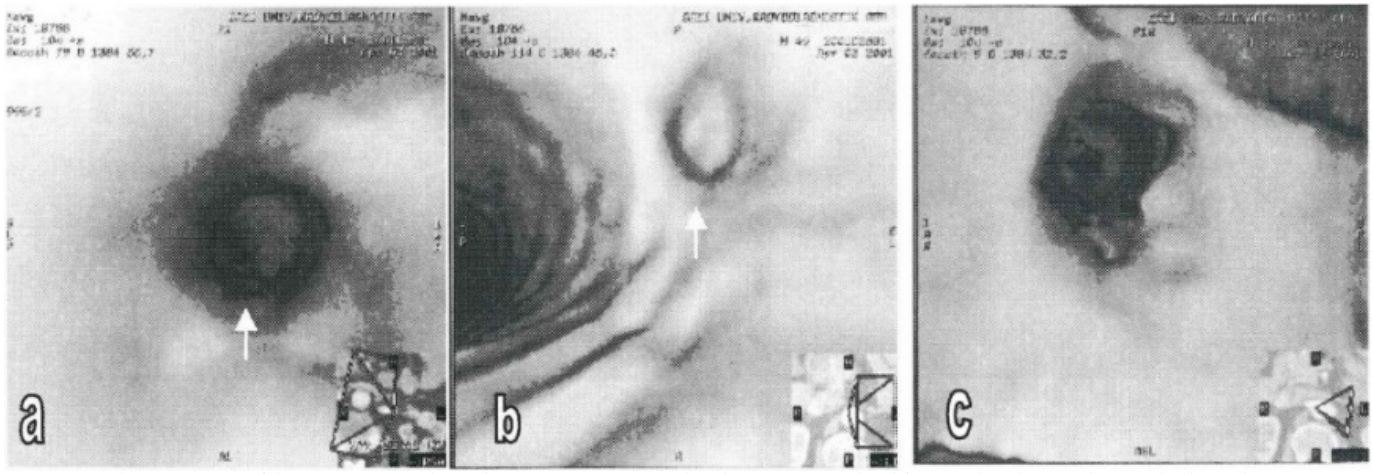


**Figure 7.** In the VIE images of the same case: (a) the occlusion (arrow) proximal to the stent is visualized from within the stent lumen, (b) the occlusion (arrow) in the proximal left renal artery is shown from the aortic lumen, and (c) the appearance of the blocked stent lumen distal to the occlusion is depicted from the aortic lumen

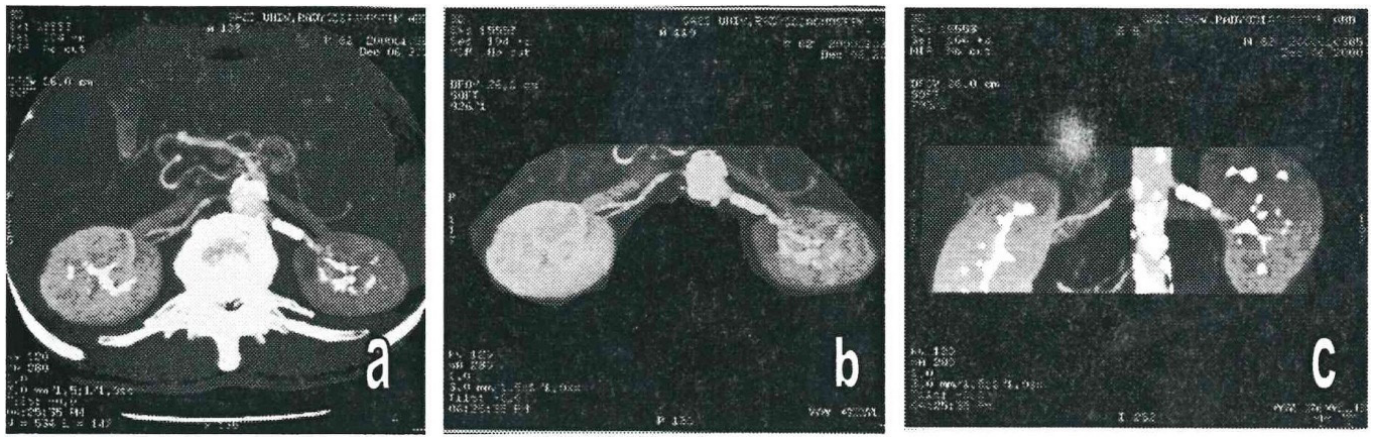


**Figure 8.** (a) The initial MIP image including the entire scanning volume is shown. After removing the bone structures, MIP images showing the entire scanning volume are presented from (b) an inferior and (c) anterior view. Windowing has been applied to visualize the vascular structures. In this case, there is up to 90% stenosis in the proximal right renal artery, and a stent is visible in the left renal artery

best results in vascular imaging are achieved when collimation finer than the diameter of the relevant vessel is used, combined with an increased pitch to enhance the scanning distance. Studies indicate that a collimation of 2 mm and a pitch of 1.5-2 are optimal for visualizing renal arteries and achieving the best image resolution.[16] In this study, for the purpose of demonstrating renal arteries and stents, 14 cases were scanned using 3 mm collimation, a table speed of 3 mm/s, and a pitch of 1:1, while 1 case utilized 3 mm collimation, a table speed of 4.5 mm/s, and a pitch of 1.5:1 (Figure 4). Therefore, the use of 3 mm collimation without increasing the pitch resulted in a slight decrease in longitudinal resolution.

During spiral CTA imaging, the patient moves in the z-axis direction (the direction of table movement), necessitating interpolation algorithms to obtain axial images from the volumetric data acquired. In reconstructions performed using the 180° linear interpolation technique, information from two angles with a 180° difference is utilized. This minimizes artifacts caused by the partial volume effect.[17] In this study, the interpolation algorithm used in the system was 180°.

In spiral CTA examinations, another important point is the use of contrast media. Sufficient arterial enhancement is necessary for a successful CTA while minimizing venous and parenchymal opacification.[18,19] This can be achieved when an appropriate scanning delay time is utilized. Delay time can be determined in three ways: First, predicting the delay time based on heart rate, blood pressure, and the patient's circulatory status; second, using small test injections; and third, employing techniques like Smart Prep (General Electric Medical Systems), which initiate scanning when an increase in attenuation is detected in the relevant vascular area. Kaatee and colleagues evaluated the delay times obtained through a fixed delay time with test injections in a group of 70 patients presenting clinical findings of renovascular hypertension and ischemic nephropathy, regarding their effectiveness in achieving maximal opacification in the renal arteries. In the first group, a fixed delay time was applied, while in the second group, they added 5, 10, 15, and 20 seconds to the time found after a test injection (15 ml of contrast medium at a rate of 3 ml/s). Statistical analysis revealed no significant difference between the two methods.[20] In our study, for visualizing the renal arteries and stents in all cases, 100-130 cc of contrast medium was administered at an injection speed of 2.5-3 ml/s, with a dosage of 1.5 cc/kg, ensuring it was not less than 100 cc. The delay times were determined as follows: 25 seconds for 7 cases, 20 seconds for 4 cases, and 10 seconds for 1 case.

In our study, all cases were processed using post-processing techniques to create MPR, MIP, SSD, and VIE images. MPR refers to coronal, sagittal, or oblique single voxel thickness planes formed by stacking axial slices. This technique is particularly effective in displaying anatomical connections that vary in any direction. In all cases, the stent was visualized separately from the intraluminal contrast. The stent appeared similar in density to the calcifications and bony structures. MPR images allow for the evaluation of the relationship, patency, and positioning of the metallic stent and vascular structures.[21]

MIP creates images by projecting imaginary rays through the reconstructed three-dimensional matrix of image data, marking the maximum attenuation value selected along each ray onto a grayscale image. The maximum attenuation value encountered by each ray is encoded into a two-dimensional projection image. The grayscale of MIP reflects relative X-ray attenuation. Additionally, the absence of a threshold value in MIP allows for the evaluation of structures with different attenuations.[21] MIP is highly sensitive in differentiating vascular calcifications from intraluminal contrast. Calcium appears five times more frequently in MIP than in SSD. Furthermore, MIP enables the differentiation of intravascular metallic stents from intraluminal contrast.[21,22] In our study, we visualized the distinction between the stent and intraluminal contrast in all cases using MIP. However, due to their high attenuation, the stent, vascular calcifications, and bony structures appeared similar in density across all cases.

In fourteen cases, the continuity of the renal artery distal to the stent was observed in thickened oblique images. In one case, MIP images showed an occlusion at the proximal stent, and due to collateral flow, the vascular structures distal to the stent were visualized. In all cases, when evaluating vascular structures using windowing in the thickened oblique MIP images obtained from the stent plane, the stent lumen could not be visualized due to its high attenuation. However, with wider windowing, the lumen was better visualized. The most significant limitation of MIP is its dependence on the degree of arterial contrast enhancement. In our study, in cases where optimal contrast enhancement could not be achieved in the renal arteries, the remaining vascular structures distal to the stent were visualized more weakly. MIP allows for the evaluation of the relationship between the metallic stent and vascular structures, as well as the position of the stent.

SSD images are created by selecting a threshold value by the user. In this process, voxels in the reconstructed three-dimensional matrix with attenuation values greater than the threshold are set to white, while those with attenuation values below the threshold are set to black, thus generating a digital image. Vascular calcification, intraluminal contrast, and the metallic stent all have attenuation above the selected threshold, resulting in these structures appearing white. Consequently, the stent lumen cannot be distinguished. Using SSD images, it is not possible to assess the stenosis or patency of the segment where the stent is placed.[23] In our study, in all cases, the stent was observed in the vascular lumen as contour overflow on SSD images, and the stent appeared similar to calcification and intraluminal contrast.

VIE is a three-dimensional perspective of digital fiber optic endoscopy.[8] It enables preoperative assessment for planning surgical or interventional treatments and serves as a non-invasive method for monitoring treatment outcomes. VIE can effectively demonstrate ostial or luminal narrowing in RAS. It allows for the differentiation of eccentrically located and calcified plaques in the ostial and distal lumen. Moreover, it provides detailed visualization of grafts or stents, assessing their position and relation to the aorta and its branches.[4,24,25] Additionally, VIE plays a significant role in demonstrating metallic prostheses within the aortic lumen, facilitating the evaluation of their patency and positioning.[26] In our study, VIE images were generated for all cases, and in 14 patients, the stent lumen was observed to be patent. In one case, occlusion at the proximal end of the stent was visualized both from the aortic lumen and the stent lumen.

Spiral CTA has the most significant advantage of being a non-invasive method, eliminating the need for arterial injection.

It is also a rapid technique, and the radiation dose used is lower.[27] However, its most notable disadvantage is the risk of contrast-induced nephrotoxicity, which increases in patients with pre-existing renal dysfunction.[28]

## CONCLUSION

Spiral CTA can be effectively used as a non-invasive method for assessing stent integrity, patency, and the relationship between the stent and renal artery following intravascular stent placement in RAS, in conjunction with scanning parameters and post-processing techniques. This provides a significant advantage in clinical applications and improves the diagnosis and treatment processes for patients.

## ETHICAL DECLARATIONS

### Ethics Committee Approval

The study was produced from a thesis before 2020, and institutional approval was received.

### Informed Consent

All patients signed and free and informed consent form.

### Referee Evaluation Process

Externally peer-reviewed.

### Conflict of Interest Statement

The author declare they have no conflicts of interest.

### Financial Disclosure

The author declared that this study has received no financial support.

### Author Contributions

The author declare that they have all participated in the design, execution, and analysis of the paper, and that they have approved the final version.

## REFERENCES

1. Gunawardena T. Atherosclerotic renal artery stenosis: a review. *Aorta (Stamford)*. 2021;9(3):95-99. doi:10.1055/s-0041-1730004
2. Prince M, Tafur JD, White CJ. When and how should we revascularize patients with atherosclerotic renal artery stenosis? *JACC Cardiovasc Interv*. 2019;12(6):505-517. doi:10.1016/j.jcin.2018.10.023
3. Borelli FA, Pinto IM, Amodeo C, et al. Analysis of the sensitivity and specificity of noninvasive imaging tests for the diagnosis of renal artery stenosis. *Arq Bras Cardiol*. 2013;101(5):423-433.
4. Tan KT, van Beek EJ, Brown PW, van Delden OM, Tijssen J, Ramsay LE. Magnetic resonance angiography for the diagnosis of renal artery stenosis: a meta-analysis. *Clin Radiol*. 2002;57(7):617-624. doi:10.1053/crad.2002.0941
5. Patel ST, Mills JL, Sr., Tynan-Cuisinier G, Goshima KR, Westerband A, Hughes JD. The limitations of magnetic resonance angiography in the diagnosis of renal artery stenosis: comparative analysis with conventional arteriography. *J Vasc Surg*. 2005;41(3):462-468.
6. Al-Rudaini HEA, Han P, Liang H. Comparison between computed tomography angiography and digital subtraction angiography in critical lower limb ischemia. *Curr Med Imaging Rev*. 2019;15(5):496-503. doi:10.2174/1573405614666181026112532
7. Klingebiel R, Kentenich M, Bauknecht HC, et al. Comparative evaluation of 64-slice CT angiography and digital subtraction angiography in assessing the cervicocranial vasculature. *Vasc Health Risk Manag*. 2008;4(4):901-907. doi:10.2147/vhrm.s2807
8. Perandini S, Faccioli N, Zaccarella A, Re T, Mucelli RP. The diagnostic contribution of CT volumetric rendering techniques in routine practice. *Indian J Radiol Imaging*. 2010;20(2):92-97. doi:10.4103/0971-3026.63043
9. Ko JP, Goldstein JM, Latson LA, et al. Chest CT Angiography for acute aortic pathologic conditions: pearls and pitfalls. *Radiographics*. 2021;41(2):399-424. doi:10.1148/rg.2021200055
10. Schoepf UJ, Costello P. CT angiography for diagnosis of pulmonary embolism: state of the art. *Radiology*. 2004;230(2):329-337. doi:10.1148/radiol.2302021489
11. Donaldson JS. Computed tomography angiography for renal artery stenosis in children: a flip flop isn't always bad. *Pediatr Radiol*. 2021;51(3):383-384. doi:10.1007/s00247-020-04873-0
12. Alam A, Chander BN. Vascular applications of Spiral CT : an initial Experience. *Med J Armed Forces India*. 2004;60(2):117-122. doi:10.1016/S0377-1237(04)80099-6
13. Brink JA, Heiken JP, Wang G, McEnery KW, Schlueter FJ, Vannier MW. Helical CT: principles and technical considerations. *Radiographics*. 1994;14(4):887-893. doi:10.1148/radiographics.14.4.7938775
14. Rubin GD, Dake MD, Semba CP. Current status of three-dimensional spiral CT scanning for imaging the vasculature. *Radiol Clin North Am*. 1995;33(1):51-70.
15. Urban BA, Fishman EK, Kuhlman JE, Kawashima A, Hennessey JG, Siegelman SS. Detection of focal hepatic lesions with spiral CT: comparison of 4- and 8-mm interscan spacing. *AJR Am J Roentgenol*. 1993;160(4):783-785. doi:10.2214/ajr.160.4.8456665
16. Brink JA, Lim JT, Wang G, Heiken JP, Deyoe LA, Vannier MW. Technical optimization of spiral CT for depiction of renal artery stenosis: in vitro analysis. *Radiology*. 1995;194(1):157-163. doi:10.1148/radiology.194.1.7997544
17. Palmaz JC, Sibbitt RR, Reuter SR, Tio FO, Rice WJ. Expandable intraluminal graft: a preliminary study. Work in progress. *Radiology*. 1985;156(1):73-77. doi:10.1148/radiology.156.1.3159043
18. Fishman EK. High-resolution three-dimensional imaging from subsecond helical CT data sets: applications in vascular imaging. *AJR Am J Roentgenol*. 1997;169(2):441-443. doi:10.2214/ajr.169.2.9242750
19. Baliyan V, Shaqdan K, Hedgire S, Ghoshhajra B. Vascular computed tomography angiography technique and indications. *Cardiovasc Diagn Ther*. 2019;9(Suppl 1):S14-S27. doi:10.21037/cdt.2019.07.04
20. Kaatee R, Van Leeuwen MS, De Lange EE, et al. Spiral CT angiography of the renal arteries: should a scan delay based on a test bolus injection or a fixed scan delay be used to obtain maximum enhancement of the vessels? *J Comput Assist Tomogr*. 1998;22(4):541-547. doi:10.1097/00004728-199807000-00008
21. Çapkan DÜ. Assessment of iliac artery stent patency using computed tomography angiography and comparison with digital subtraction angiography. *Chronicles Precis Med Res*. 2024;5(2):70-73.
22. Zhang L, Li L, Feng G, Fan T, Jiang H, Wang Z. Advances in CT techniques in vascular calcification. *Front Cardiovasc Med*. 2021;8:716822. doi:10.3389/fcvm.2021.716822
23. Addis KA, Hopper KD, Iyriboz TA, Kasales CJ, Liu Y, Wise SW. Optimization of shaded surface display for CT angiography. *Acad Radiol*. 2001;8(10):976-981. doi:10.1016/S1076-6332(03)80641-4
24. Skutta B, Furst G, Eilers J, Ferbert A, Kuhn FP. Intracranial stenoocclusive disease: double-detector helical CT angiography versus digital subtraction angiography. *AJNR Am J Neuroradiol*. 1999;20(5):791-799.
25. De Cobelli F, Vanzulli A, Sironi S, et al. Renal artery stenosis: evaluation with breath-hold, three-dimensional, dynamic, gadolinium-enhanced versus three-dimensional, phase-contrast MR angiography. *Radiology*. 1997;205(3):689-695. doi:10.1148/radiology.205.3.9393522
26. Urbanik A, Skladzień J, Chrzan R, Popiela T, Wojciechowski W. Virtual endoscopy CT and three-dimensional reconstruction CT: new possibilities in middle ear diagnostics. *Rivista di Neuroradiologia*. 2001;14(6):639-646.
27. Ruiz-Cruces R, Perez-Martinez M, Martin-Palanca A, et al. Patient dose in radiologically guided interventional vascular procedures: conventional versus digital systems. *Radiology*. 1997;205(2):385-393. doi:10.1148/radiology.205.2.9356618
28. Parfrey PS, Griffiths SM, Barrett BJ, et al. Contrast material-induced renal failure in patients with diabetes mellitus, renal insufficiency, or both. A prospective controlled study. *N Engl J Med*. 1989;320(3):143-149. doi:10.1056/NEJM198901193200303